

Enabling Si-Dominant Anodes: Influence of Neutralization Degree of Polyacrylic Acid on Low-Cost Micron-Sized Silicon Anode in High-Energy Li-Ion Full Cell

Gabriele Kloker,^{*[a, c]} Dragoljub Vrankovic,^[a] Nikhil Arya,^[c, d] Thomas Diemant,^[d] and Montaha Anjass^{*[b, c, d]}

Micron-sized silicon is a promising low-cost, abundant material to increase the energy density of lithium-ion batteries. Nevertheless, significant volume change and therefore excessive solid electrolyte interphase (SEI) growth lead to fast capacity fading. In this work, polyacrylic acid (PAA) with different neutralization degrees is used for the fabrication of Si anodes for practical applications. The electrochemical performance in full pouch cells reveals that the increase in neutralization degree of PAA up to 70% enhances the overall performance by improved electrode properties, higher first cycle efficiency (FCE up to 78.1% at C/3) and better capacity retention (85.4% after 150

cycles at 1 C) over cycling, while with even higher neutralization degrees (such as 80%) the performance declines. Since proper mixing of the slurry is another important factor, we optimized the mixing procedure by increasing the solid content of the slurry, which has shown positive influence on the electrochemical performance and electrode properties. To summarize, this work shows full cell 1 C cycling until capacity retention of 85% after 150 cycles with pure Si microparticle anodes for 70% neutralized PAA as well as increased C-rate performance up to 5 C. Post-mortem, less degradation on electrode and particle level is observed.

1. Introduction

Silicon (Si) possesses a high theoretical capacity of $>3500 \text{ mAh g}^{-1}$ at room temperature, which is almost ten times higher than graphite (372 mAh g^{-1}), and a low discharge potential of about 0.37 V with respect to lithium metal. Together with its abundance, environmental friendliness and low cost, it is recognized as next-generation anode material for lithium-ion batteries (LIBs).^[1–5] Nevertheless, metallurgical micron-sized Si has not yet been investigated to large extent due to numerous intrinsic issues. Foremost significant volume expansion of Si during the lithiation process of more than 300% causes cracks formation throughout the particle and electrode as well as loss of electrical contact with the current

collector and between particles. Moreover, excessive solid electrolyte interphase (SEI) growth due to continuous exposure of fresh active material surface to electrolyte leads to loss of active lithium (Li) due to side reactions^[1,2,5,6] and Li trapping.^[7–9] In order to enable the application of Si in industrial cells to boost energy density, several strategies were followed and investigated in detail. Most prominent has been using nanostructures, surrounding Si with a shield of carbon or developing new binder systems.^[2,5,6,10–13] Up to now, most studies still focus on electrodes based on Si and graphite with different ratios, often containing only low amount of Si nanoparticles (SiNPs) in order to avoid the fracturing of the particles.^[14–16] Even though nanoparticles prevent particle cracking, the enlarged surface area leads to more electrolyte degradation and therefore lower first cycle efficiency (FCE). Electrode processing, especially proper mixing, is also tedious and results in electrodes with low density.^[14] In contrast, Si microparticles (SiMPs) offer a cost-effective alternative with higher tap density, less side reactions due to reduced surface area and easier processing. However, increased internal strain and therefore particle fracture is the main drawback in comparison to SiNPs.^[17] Therefore, custom-fit binder systems as mitigation strategy are especially important for SiMP-based anodes. A big variety of different approaches has already been described in literature, leading from the more commonly used linear binders like polyacrylic acid (PAA), over cross-linked binders to systems with self-healing ability. In all cases the main requirements for industrial application are low cost and aqueous processing.^[18–22] The most prominent binder used for Si anodes is PAA, which offers abundant carboxyl (COOH) groups that can interact with the functional groups of the Si surface such as silanol (Si–O–H) groups. An important modification is the partial neutralization of PAA, which

[a] G. Kloker, D. Vrankovic
Mercedes-Benz AG, Mercedesstraße 130/6, 70327 Stuttgart, Germany
E-mail: gabriele.kloker@mercedes-benz.com
gabriele.kloker@uni-ulm.de

[b] M. Anjass
University of Sharjah, Department of Chemistry, Sharjah-27272 Sharjah, United Arab Emirates
E-mail: malmasri@sharjah.ac.ae

[c] G. Kloker, N. Arya, M. Anjass
Ulm University, Institute of Inorganic Chemistry I, Albert-Einstein-Allee 11, 89081 Ulm, Germany

[d] N. Arya, T. Diemant, M. Anjass
Helmholtz Institute Ulm (HIU), Helmholtzstr. 11 89081 Ulm, Germany
Supporting information for this article is available on the WWW under <https://doi.org/10.1002/batt.202400330>

© 2024 The Authors. Batteries & Supercaps published by Wiley-VCH GmbH. This is an open access article under the terms of the Creative Commons Attribution License, which permits use, distribution and reproduction in any medium, provided the original work is properly cited.

influences the properties strongly. Not only the chemical interaction changes, but also the conformation of the polymer, therefore the homogeneity of polymer around the particles.^[23–26] A further important aspect is the ratio of Si to graphite inside the electrode, as this affects the interaction with the binder enormously. A small ratio of Si within the active material of the anode will not help to push boundaries for energy density and will affect the understanding of the interaction between PAA and Si. In such anodes the majority of the active material is graphite, which behaves differently with PAA than Si, what also reveals in the electrochemical data, as PAA is not an optimum binder for graphite.^[27] Those effects may overlap the influence on the electrochemistry originating from the interaction of PAA with Si. While most literature states how PAA and lithiated/neutralized PAA (Li_xPAA) is acting in the electrode and how it is expected to be distributed around the Si particles, this work actually visualizes the binder using transmission electron microscopy - electron energy loss spectroscopy (TEM-EELS), even though the binder has no specific heteroatoms to enable detection via the common analytical methods. In addition, the influence of the neutralization degree on the electrochemical performance and degradation is studied in detail in both half and full cell in this work.

In total, this work shows an optimized pure micron-sized Si anode with industrial-relevant composition and loading, which features a drastically improved overall performance with higher neutralization degree of the PAA until $\text{Li}_{0.7}\text{PAA}$, as shown in electrode properties and electrochemical data.

2. Results and Discussion

Silicon, being an abrasive material with a surface offering a large amount of functional groups, allows for significantly more interactions with the other components in the slurry (such as binder) while also preventing agglomerates from being destroyed by conventional methods during electrode processing. First, we tested the effect of solids content (SC) during the mixing phase on the electrochemical performance of samples with the $\text{Li}_{0.3}\text{PAA}$ binder. The mentioned SC during mixing means the highest SC within the mixing procedure, which occurs after the addition of all the silicon and carbon black to the binder solution, before adding the SWCNTs and diluting the slurry for better coating ability. For the tests, either low SC (approx. 50%) or high SC mixing (approx. 64%) were used. Figure 1a reveals that by increasing the SC during mixing the capacity retention got improved by almost 10% (from 72.9%–82.5%) at 150th cycle at C/3 rate. Interestingly, the SC during preparation also had influence on the C-rate performance, viz., the electrodes with higher SC showed slightly higher capacities for all C-rates with stronger effect for higher C-rates (Figure 1b).

The neutralization of PAA helps in a large extend to ease processing of the pure Si anode slurry regarding viscosity/rheological properties. Nevertheless, it needs to be considered that also the pH of the slurry rises with increasing neutralization degree of the PAA, as the Li^+ ions of the dissolved LiOH interact with the carboxylic acid groups of the PAA forming COOLi , at

the same time leaving OH^- anions into the solution. Hydrogen formation is enabled and accelerated with increasing pH based on the reactions at the Si surface, meaning dissolution of the silica hydrogel and therefore facilitated hydrolysis of Si. Furthermore, the oxidation of Si can be additionally accelerated in presence of carbon black.^[28,29] Overall, these effects can lead to reduced stability of the slurry especially in larger batches due to gassing. However, the effect is reduced for SiMPs due to lower surface area ratio. The change in processing of the pure silicon anode slurry originates from the different interactions between binder and particles/substrate, and both influence the electrode properties, therefore the adhesion is one measure to show the differences. The results of the 90° peel test in Figure 2a show an increasing adhesion with increased partial neutralization of PAA. Previous work^[30] showed that the interaction between binder and copper current collector is reduced with higher neutralization degree, while this work showed a higher adhesion for the electrodes with higher neutralization degree. On the one hand this might be counter-intuitive, as the partial neutralization prevents a corresponding amount of carboxylic acid groups from bonding with the particle surface groups and substrate, on the other hand this observed trend fits together with the explanation of polymer conformation, meaning stretched and decoiled PAA chains due to partial neutralization.^[31,32] The change to a stretched conformation of the polymer would then lead to a much higher interaction ability between polymer chain and surface as in a coiled conformation where most functional groups are blocked by intramolecular interactions. Additionally, the type of bonding is changed due to changes in the pH value.^[23,26] Therefore, more chemical bonds are formed than in acidic conditions. Also, the comparison between samples with different SC surprisingly shows lower adhesion for the $\text{Li}_{0.3}\text{PAA}$ with high SC, almost as low as for the acidic sample. The binder distribution/influence seems to be quite different in those two cases, as the cohesion contrariwise is higher for the sample mixed with high SC, and even higher as for the more neutralized samples, where the cohesion seems to even decline slightly with higher neutralization degree. Together with the differences in electrochemical performance between the two different mixing routines, cohesion seems to be the more influencing factor than adhesion. Next, we measured the electronic resistivity at room temperature on three different spots of each electrode using a Hioki device. In order to avoid randomness in laboratory mixing, both adhesion and electronic resistivity were measured not only with three samples of one electrode, but also with different coatings on different days to assure repeatability. As shown in Figure 2b the interface resistances between coating and copper substrate are comparable for $\text{Li}_{0.3}\text{PAA}$ ($0.0081 \Omega \text{cm}^2$) and $\text{Li}_{0.7}\text{PAA}$ ($0.0042 \Omega \text{cm}^2$), while the one for Li_0PAA ($0.055 \Omega \text{cm}^2$) is much higher, and $\text{Li}_{0.8}\text{PAA}$ ($0.031 \Omega \text{cm}^2$) is lying in between. Notably, the interface resistance for the $\text{Li}_{0.3}\text{PAA}$ containing electrode with high SC of $0.0045 \Omega \text{cm}^2$ is as low as the one of $\text{Li}_{0.7}\text{PAA}$ ($0.0042 \Omega \text{cm}^2$) with standard mixing. While the interface resistance of $\text{Li}_{0.7}\text{PAA}$ seems to be most beneficial, it changes when checking the composite volume resistivity. In this case, electrodes with Li_0PAA ($0.835 \Omega \text{cm}$) and $\text{Li}_{0.3}\text{PAA}$

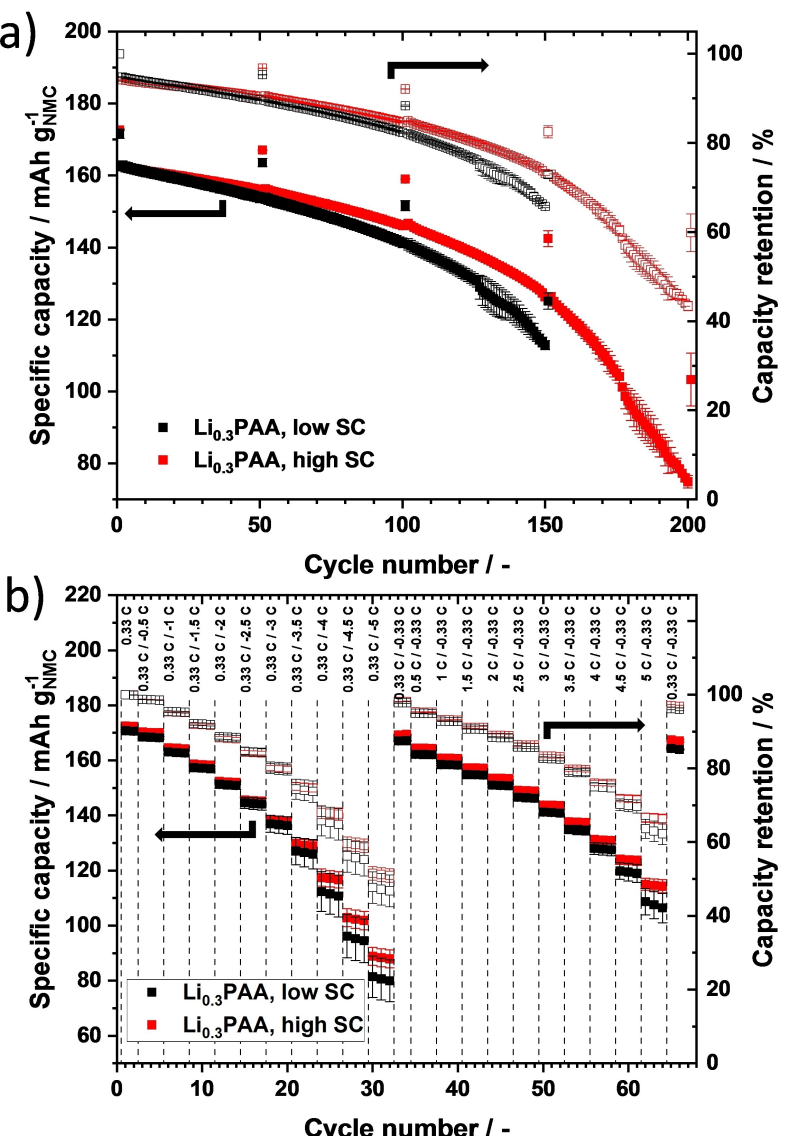


Figure 1. Electrochemical performance of Li_{0.3}PAA-containing electrodes with different solids contents during mixing (low SC ~50% and high SC ~64%). **a)** Capacity retention at 1 C cycling with C/3 check-up cycles each 50th cycle and **b)** C-rate performance in Si || NMC811 full pouch cell. The C-rates given on top of the graph show the variation of the discharge rate in the first half and variation of the charge rate in the second half of cycles. The charge rate in the first half and the discharge rate in the second half were kept constant at C/3. The end of the test consists of C/3 cycles to check how well the initial capacity is maintained.

(0.802 Ω cm) show the lowest composite volume resistivity, which increases for Li_{0.3}PAA with high SC and Li_{0.7}PAA, offering the highest values of 1.499 Ω cm and 2.052 Ω cm, respectively. Finally, the Li_{0.8}PAA containing electrode does not follow the trend, as its value (1.489 Ω cm) is slightly lower than Li_{0.7}PAA, but still higher than the value of Li₀PAA and Li_{0.3}PAA. As this effect is expected to be mostly influenced by the conductive additives' dispersion, it will be discussed in more detail later. Therefore, based on the measured resistances, especially for interface resistances clear overall improvements are shown by using partially neutralized PAA in comparison to Li₀PAA. Among the different neutralization degrees, Li_{0.3}PAA shows the optimum combination of respective interface and composite volume resistivity.

To get an overview of the surface morphology of the silicon electrodes with different partial neutralization of the binder, scanning electron microscope focused ion beam (SEM FIB)-cross section images were recorded. Figure S1 shows the morphology of pristine electrodes. It can be seen that due to slight calendering the surface of the electrodes is quite smooth and homogenous, as well the distribution of silicon particles, but still not so densified that the porous electrode structure is lost. At some spots the carbon black looks agglomerated, which is known as well for pure graphite electrodes. There are no major differences observed in the different samples.

In order to comprehend the properties and performance of the anode depending on variations in the degree of neutralization of PAA, it is essential to gain an understanding of the

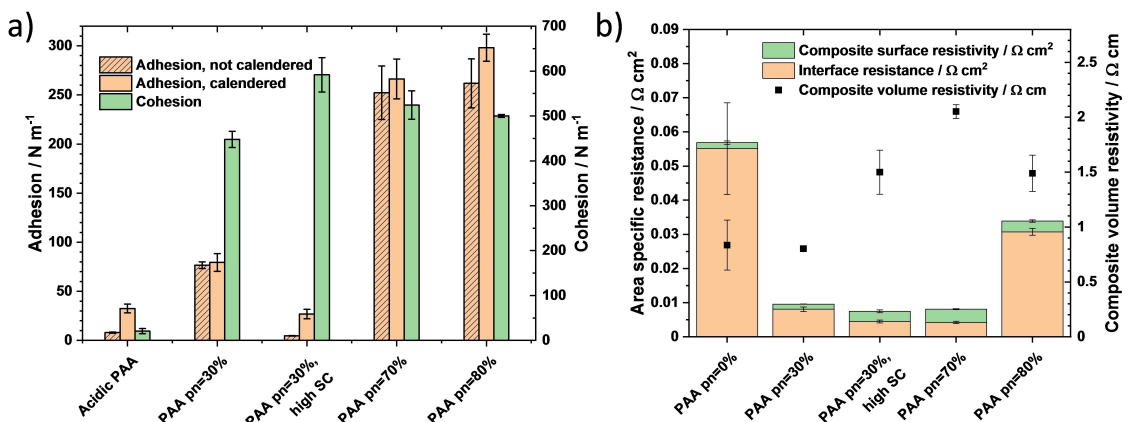


Figure 2. a) Adhesion of non-calendered (orange, shaded) and calendered (orange) electrodes with different PAA neutralization degree and cohesion (green), all measured in 90° peel tests. b) Measured resistances of calendered electrodes with different PAA neutralization degree showing composite surface resistivity (green) and interface resistance (orange) as bars and composite volume resistivity as dots (black).

particle-binder interaction. Although it has been demonstrated in literature how the interaction changes with variation of the pH value or neutralization degree, more research is still required to gain more insight into the particle-binder interaction. Since this binder does not contain any heteroatom to distinguish it from the carbon of carbon additives and the oxygen and hydrogen of the native oxide layer on the Si surface, the usage of SEM-EDX is not suitable for that purpose and the analytical techniques to investigate the particle-binder interaction are limited. CryoTEM-EELS is a potential technique, that offers a differentiated view on the respective elements based on their (bonding) state. In this work, cross-section TEM-EELS spectrum mapping images for the Li₀PAA, Li_{0.3}PAA and Li_{0.7}PAA containing electrodes were collected. During mapping, it is possible to distinguish between the different states of carbon in carbon black and binder, demonstrating the uniformity of the binder coating around the particle. Furthermore, the oxygen state can be distinguished between oxygen at the interface and oxygen in the bulk of the binder in principle. Unfortunately, the signal was rather noisy due to overlapping signals in our case. Therefore, the different oxygen states could not be mapped reliably. Nevertheless, the mapping of the carbon assigned to the binder enables us to draw conclusions about the structural differences of the samples with different neutralization degree. The cross-section TEM images of the Li₀PAA electrode shown in Figure 3a give insight into the binder/conductive additive phase between the silicon particles. Not only the elemental distribution of silicon, carbon and oxygen is shown, but as well the different states of carbon (Figure 3b), which can be attributed to carbon black and binder by EELS spectra (Figure 3c). Based on that, the binder looks to be rather inhomogeneously distributed and especially concentrated around the carbon black instead of a homogenous distribution on the silicon particle surface. This is also visible in another part of the same electrode, shown in Figure S2. Therefore, carbon black agglomerates in the space between the particles, forming conductive paths, which are weakly attached to the Si particles. Nevertheless, they may could lead to a conductive network in

between the particles, resulting in lower composite volume resistivity for Li₀PAA as shown in Figure 2b, but inefficient conductive particle connection.

In contrast, the cross-section TEM-EELS results of Li_{0.7}PAA (Figure 4) show that the carbon attributed to carbon black is embedded in the one assigned to the binder, the latter simultaneously appearing to be homogeneously covering the Si particle surface. Hence, this technique allows to compare the distribution of the binder in electrodes with different binder modifications, concluding that the partial neutralization of PAA leads to a more homogenous distribution around the silicon particles due to the decoiled, stretched conformation.^[31,32] In addition, the carbon black accumulation by the binder seems to be much reduced with partial neutralization of the binder, leading to higher composite volume resistivities as shown in Figure 2b, but also conductive paths attached to the Si particles, therefore efficiently connecting Si particles. Finally, a similar investigation of the Li_{0.3}PAA electrodes (Figure S3), shows an intermediate result between both extremes. It should be noted that due to the porous nature of the pure Si anode the sample preparation gets much more complicated, as the generated lamella need to be thinned, causing breaking off from parts of the structure. Therefore, the images seem to include a lot of voids, which is the result of the remaining part of thin lamella. For mapping the different (bonding) states of oxygen the resolution of this method is too low. Therefore, we further studied the electrodes by using X-ray photoelectron spectroscopy (XPS) to gain insight into the elemental composition and distinguish between the different states of oxygen.

XPS survey spectra of the pristine Li₀PAA, Li_{0.3}PAA and Li_{0.7}PAA electrodes show peaks corresponding to C, O, and Si as major components (Figure S4). In addition, a small Cu contribution (from the Cu foil) could also be detected in some cases. The Si 2p detail spectra in Figure S5 (left column) of the Li₀PAA, Li_{0.3}PAA and Li_{0.7}PAA electrodes show three features which can be assigned to elemental Si⁰ (Si 2p^{3/2} peak at binding energy of 99.0 eV), intermediate SiO_x (100.5 eV) and SiO₂ (103.1 eV).^[33,34] Comparison of the three Si 2p spectra shows a significant

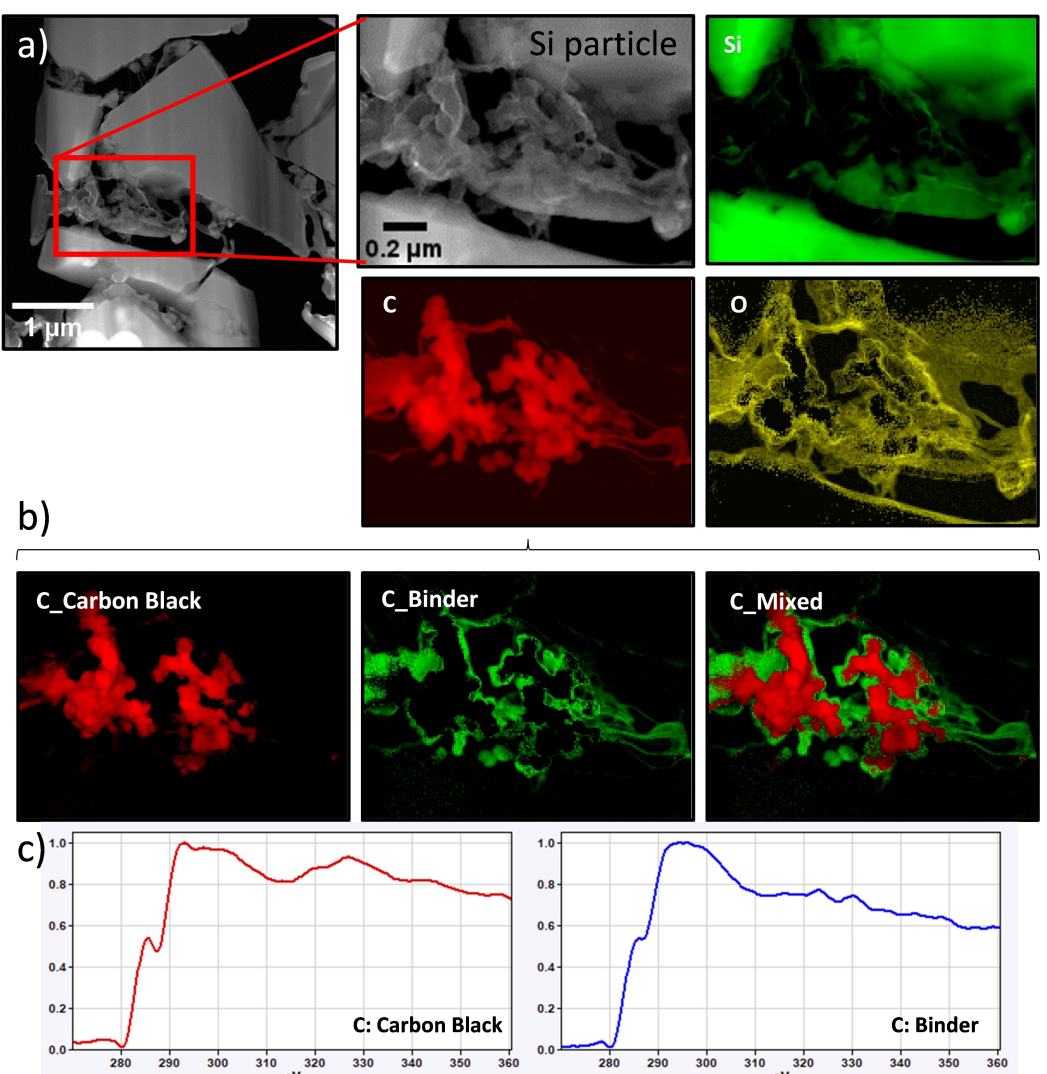


Figure 3. a) Cross-section TEM image of the Li_0PAA electrode showing Si particles and the binder/conductive additive mixture in between with the elemental mapping of silicon (green), carbon (red) and oxygen (yellow). b) Differentiated carbon states by EELS for carbon black (red) and binder (green). c) Spectra for carbon which can be attributed either to carbon black or PAA binder.

reduction of the intensity for $\text{Li}_{0.3}\text{PAA}$ and $\text{Li}_{0.7}\text{PAA}$ compared to Li_0PAA . The Si species show slightly higher ratio of $\text{SiO}_x/\text{SiO}_2$ for the partially neutralized samples due to higher pH value during slurry fabrication. The reduced general intensity of the Si 2p peaks for the partially neutralized samples can be explained by the more homogeneous coverage of the Si particle by the binder, this can be also observed in the O 1s region with reduced SiO_2 contribution for the partially neutralized samples and fits to the conclusion drawn from the TEM-EELS. Four contributions can be discerned in the C 1s spectra (Figure S5, middle column), which can be assigned to conductive carbon (284.4 eV), as well as C–C/C–H (285.0), C–O (286.3 eV) and O–C=O (288.8 eV) species.^[33–35] A clear increase of the C–O contribution can be observed with increasing neutralization, while the O–C=O signal stays almost constant. Furthermore, a change of the main C contribution from the signal of C–C/C–H to conductive carbon occurs with increasing neutralization, which could be a result of the changing interaction between

(neutralized) binder and conductive carbon. Finally, the spectra in the O 1s region (Figure S5, right column) reflect more or less the findings of the measurements in the Si 2p and C 1s region. First, the reduction of the SiO_2 signal in the Si 2p spectra of $\text{Li}_{0.3}\text{PAA}$ and $\text{Li}_{0.7}\text{PAA}$ translates to the intensity of the corresponding peak in the O 1s spectra at 532.6 eV. Second, an increase in the O–C peak intensity is observed with increasing neutralization.^[34–36]

Even though the interaction of particles with binder is challenging to analyze, the variation of the neutralization degree of the binder has quite pronounced consequences for the electrochemical behavior. The electrochemical properties of Li_0PAA , $\text{Li}_{0.3}\text{PAA}$ and $\text{Li}_{0.7}\text{PAA}$ electrodes were investigated in coin-cell configuration with Si anode against Li metal, cycling between 0.01–1.5 V vs Li^+/Li at C/3 (after formation) in three cells to test reproducibility. A comparison of voltage profile and FCE for the Si electrodes with different degree of PAA neutralization (Figure 5) reflects the variation in SEI formation.

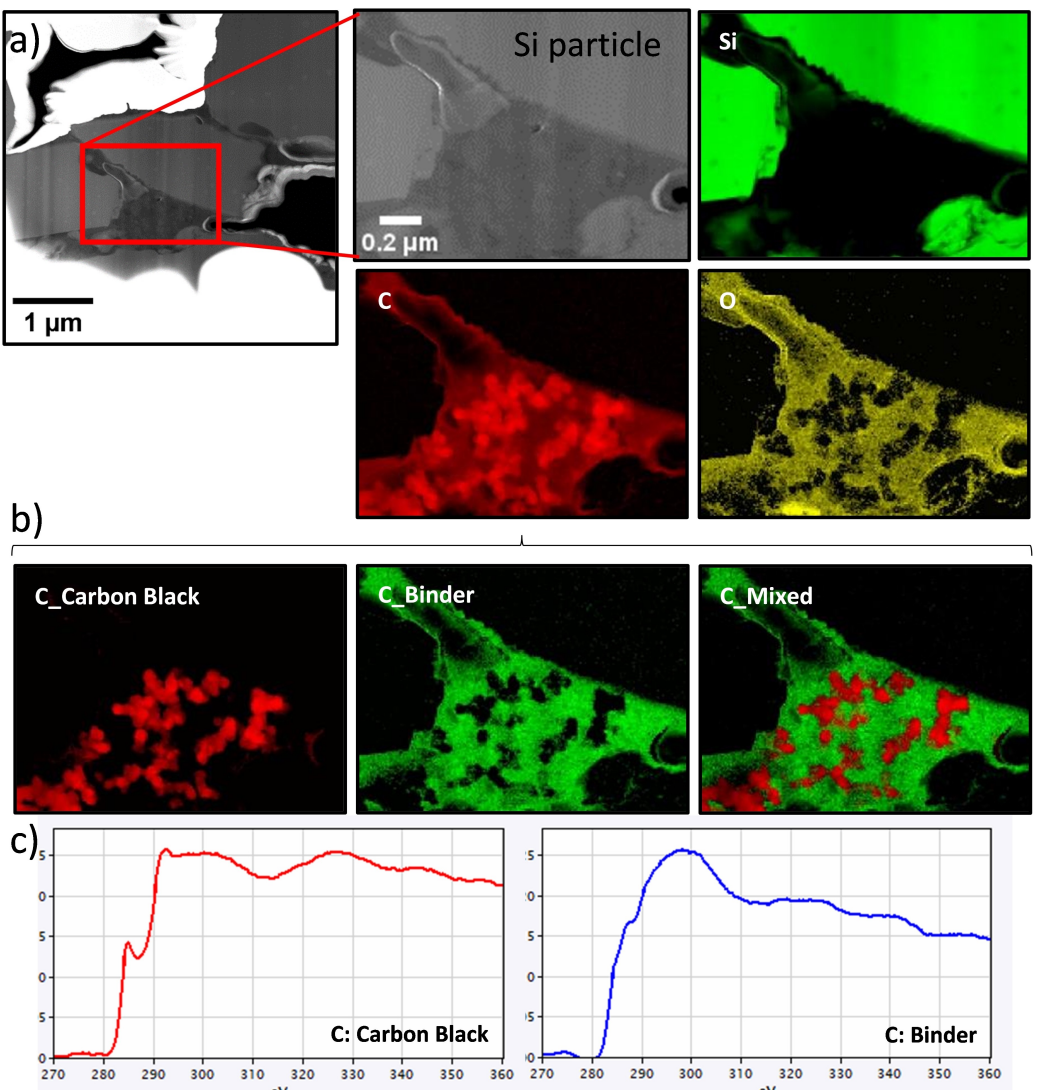


Figure 4. a) Cross-section TEM images of the $\text{Li}_{0.7}\text{PAA}$ electrode showing Si particles and the binder/conductive additive mixture in between with the elemental mapping of silicon (green), carbon (red) and oxygen (yellow). b) Differentiated carbon states by EELS shown for carbon black (red) and binder (green) c) Spectra for carbon which can be attributed either to carbon black or PAA binder.

While the FCE of the Li_0PAA electrodes in half cells is 89.3%, it increases to 92.2%, 94.4% and 94.9% for $\text{Li}_{0.3}\text{PAA}$, $\text{Li}_{0.7}\text{PAA}$ and $\text{Li}_{0.8}\text{PAA}$ electrodes, respectively. Amongst others this trend can be attributed to less electrochemical lithiation of the binder during first cycle.^[34,37] Therefore, the partial neutralization has a beneficial influence on the SEI formation in the first cycle, while leading to less consumption of active Li within the cell than Li_0PAA , where the lithiation happens fully electrochemically. This can be seen in the respective voltage range for SEI formation during Si lithiation, which shows a changed capacity profile. The beneficial SEI properties based on partial neutralization of the binder also go beyond the first cycles. The half-cell cycling with limited capacity of $1500 \text{ mAh g}_{\text{Si}}^{-1}$ in Figure 5e shows stable cycling for all electrodes with different neutralization degrees. However, the cumulative irreversible capacity shows a quite differentiated picture of the different binder modifications. While for the Li_0PAA electrode, the cumulative

irreversible capacity increases quite linearly and much more than for the rest, the partially neutralized ones show less cumulative irreversible capacity with a short increase in the beginning, then much reduced increase during cycles 10–20, followed by an increase again. Both $\text{Li}_{0.3}\text{PAA}$ and $\text{Li}_{0.7}\text{PAA}$ show the same development, but with lower values for $\text{Li}_{0.7}\text{PAA}$, showing a smaller Li loss not only in the beginning for the SEI formation, but overall cycles. Interestingly, the $\text{Li}_{0.8}\text{PAA}$ electrode does not show the plateau with distinct reduced increase, but more of a constantly growing cumulative irreversible capacity, ending up with roughly the same values after 30 cycles like $\text{Li}_{0.3}\text{PAA}$, therefore showing no distinct stabilization. Based on that, it looks like the increasing partial neutralization does not lead to a linear improvement of beneficial properties, therefore the improved performance cannot be only attributed to the increased lithium-ion amount in the binder. Half-cell C-rate tests were conducted as well (Figure S6), giving a small

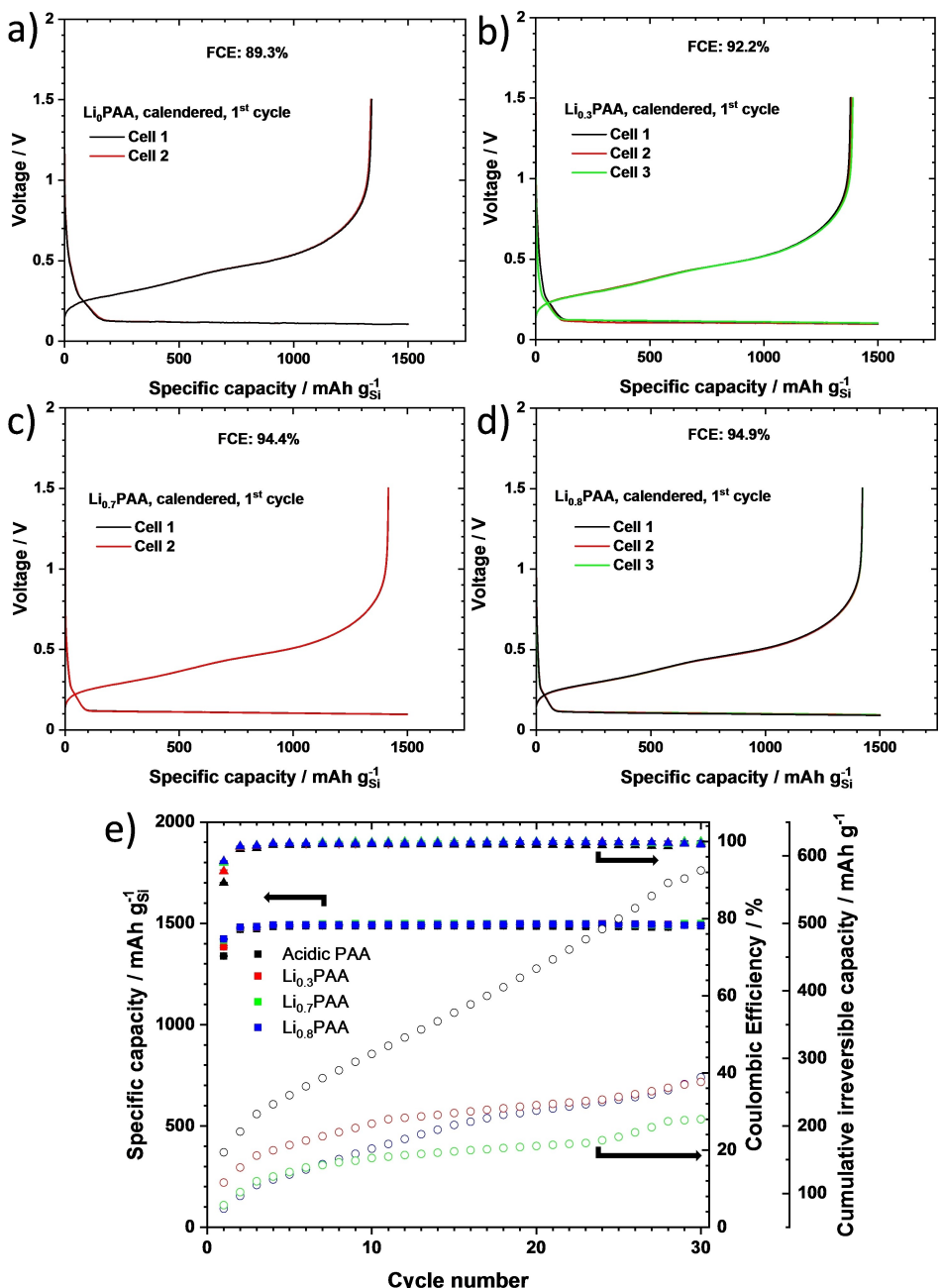


Figure 5. First cycle of half cells with Si anodes containing PAA binder with different neutralization degree (a) Li_0PAA , (b) $\text{Li}_{0.3}\text{PAA}$, (c) $\text{Li}_{0.7}\text{PAA}$ and (d) $\text{Li}_{0.8}\text{PAA}$. Tested against Li metal in the range of 0.01–1.5 V vs Li^+/Li at C/20 first formation. e) Specific capacity (triangles) and cumulative irreversible capacity (circles) of half-cells with Si anodes containing Li_0PAA (black), $\text{Li}_{0.3}\text{PAA}$ (red), $\text{Li}_{0.7}\text{PAA}$ (green) and $\text{Li}_{0.8}\text{PAA}$ (blue) at limited charge capacity of 1500 mAh g⁻¹.

glimpse on the influence of partial neutralization on the fast charge behavior, but due to the stronger overpotentials at high currents on lithium metal the results are not as reliable.^[38] To understand the electrode stability, and other properties of the electrodes better, full cell cycling was conducted in small pouch cells.

The positive influence of increasing partial neutralization on the FCE directly transfers to full-cell measurements, where the same FCE increase between Li_0PAA , $\text{Li}_{0.3}\text{PAA}$, $\text{Li}_{0.7}\text{PAA}$ and $\text{Li}_{0.8}\text{PAA}$ is observed like in the half-cell measurements. In full cell a maximum FCE of ~80% in the first formation cycle is

reached for the $\text{Li}_{0.8}\text{PAA}$ variation, which is comparable to literature, when taking into account the narrower voltage range of 3–4.2 V vs Li^+/Li used in this work.^[39–41] As can be seen in the first formation cycle of the respective variations shown in Figure 6, the difference in SEI formation is clearly visible with faster increasing voltage upon lithiation of the anodes with higher neutralization degree of the PAA.

While taking into account, that due to 100% ratio of silicon as active material significant electrolyte degradation takes place in the first cycle, it nevertheless gives a fast rise of CE in the next few following cycles. The cycle life test at 1 C with C/3

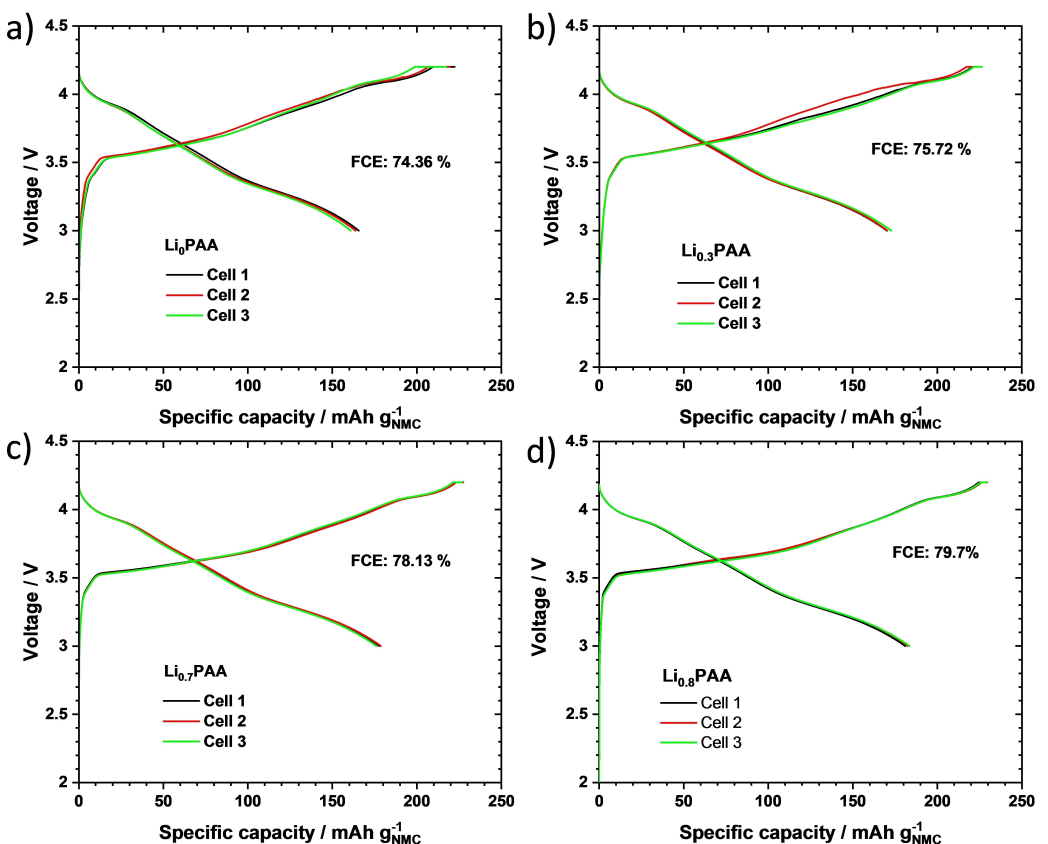


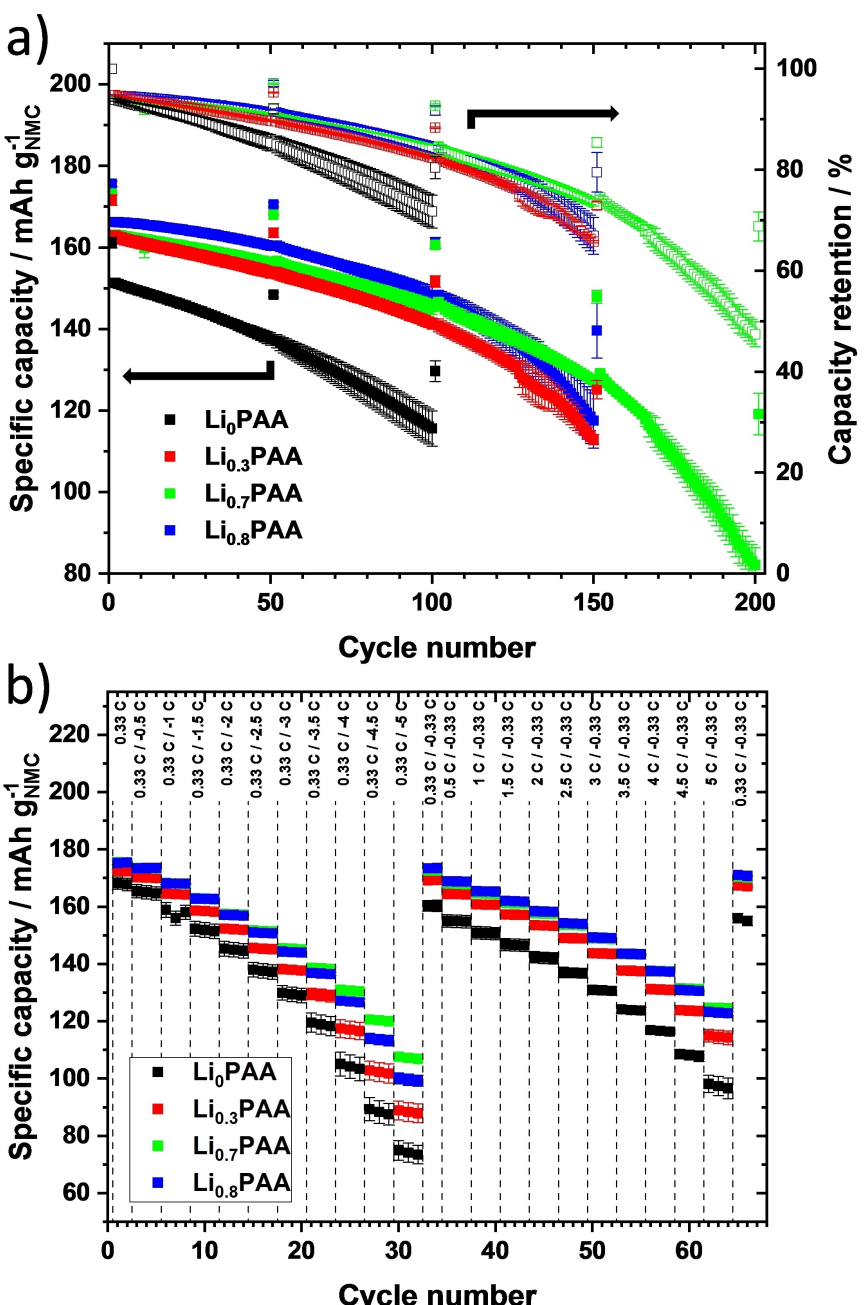
Figure 6. First formation cycle of full cells with Si anodes containing PAA binder with different neutralization degree (Li_0PAA , $\text{Li}_{0.3}\text{PAA}$, $\text{Li}_{0.7}\text{PAA}$ and $\text{Li}_{0.8}\text{PAA}$). Measured in full pouch cells against NMC811 cathodes in a voltage window of 3.0–4.2 V vs. Li^+/Li at C/10.

check-up cycles each 50th cycle shown in Figure 7a shows that the partial neutralization helps substantially to enlarge the capacity retention. While the Li_0PAA -based electrodes allow cycling only up to 100 cycles until $\text{SOH}=80\%$ is reached, the $\text{Li}_{0.3}\text{PAA}$ and $\text{Li}_{0.8}\text{PAA}$ electrodes reach 150 cycles and $\text{Li}_{0.7}\text{PAA}$ 200 cycles until that threshold. However, all of the synthesized electrodes undergo fast degradation after that point and eventually break down.

To gain further insights into the performance of the respective electrodes, a C-rate test was conducted with C-rate variation first in discharge direction, then in charge direction. As it can be seen in Figure 7b, the electrodes based on higher neutralization degree show better performance in both discharge and charge C-rate variation. Interestingly, the $\text{Li}_{0.8}\text{PAA}$ -based electrode shows slightly lower performance in the fast-charging test, but even more pronounced in the discharge direction compared to the best-performing $\text{Li}_{0.7}\text{PAA}$. The electrode properties shown in Figure 2 indicate not only worse adhesion, but also higher resistivity values for $\text{Li}_{0.8}\text{PAA}$ compared to Li_0PAA . This could be causing the lower C-Rate performance. Even though $\text{Li}_{0.3}\text{PAA}$ shows better resistivity values than $\text{Li}_{0.8}\text{PAA}$, this is most probably based on the already described carbon black agglomeration, leading to an inefficient conductive network, which doesn't connect active material particles beneficially. For that reason, $\text{Li}_{0.8}\text{PAA}$ with rather stretched PAA conformation and resulting less agglomerated

conductive additives offers better C-Rate performance than $\text{Li}_{0.3}\text{PAA}$. Nevertheless, the C/3 capacity retention after the C-rate variation test in Figure 7b shows that the Li_0PAA electrode cannot maintain the initial capacity at C/3 and shows a much faster degradation than the $\text{Li}_{0.7}\text{PAA}$ electrode, which still provides almost the same C/3 capacity after the C-rate variation test.

After the standard cycling test in Figure 7a, the post-mortem analysis was performed to investigate the morphological and structural changes of the used electrodes at $\text{SOH}=70\%-80\%$ with SEM-EDX, as shown in Figure S7 (SEM) and Figure S8 (EDX mapping). Based on top view SEM images of the electrodes in Figure S7a it can be seen that with increasing neutralization degree the number of cracks increases, but the intensity of the cracks gets less, meaning that they are finer. In FIB cross-sections of the cycled electrodes in Figure S7b, one can clearly observe severe degradation of the Li_0PAA electrode, not only showing cracks, but even voids throughout the electrode thickness. The $\text{Li}_{0.3}\text{PAA}$ electrode already shows less distributed damage across the electrode, but even though there are no voids visible, the cracks are still severe. The cross-section image of the $\text{Li}_{0.7}\text{PAA}$ electrode reveals a mild damage and only fine cracks are visible within the coating, but unlike the Li_0PAA electrode, no delamination of the coating from the current collector is observed. The cross-section images also reveal different ageing of the particles throughout the electrode and



can indicate more inorganic SEI for higher neutralization degrees.

In the next step, XPS measurements were also conducted with the cycled electrodes to get more insight into the elemental composition and the chemical species in the top layer of the SEI. The corresponding results are presented in Figure S10 and S11. The XPS survey spectra in Figure S10a show peaks for C and O from the binder, but as well from degradation products of the organic electrolyte solvents. P and F signals can be observed, which can be attributed to the electrolyte salt (LiPF_6) and its decomposition products, the electrolyte additive fluoroethylene carbonate (FEC) is another potential F source. Coming to the detail spectra, a pronounced reduction of the intensity is observed in the Si 2 p region (Figure S11a) for the cycled compared to the pristine samples of Li_0PAA , $\text{Li}_{0.3}\text{PAA}$ and $\text{Li}_{0.7}\text{PAA}$, which indicates the formation of a SEI layer with an average thickness of several nanometers (i.e., slightly less than the sampling depth of the XPS experiment). Furthermore, it is interesting to note that an additional feature is detected at lower binding energy (Si 2p_{3/2} peak at 96.2 eV) for all samples, which is most probably related to Si–Li alloy(s). On the other hand, the feature due to SiO_2 disappears at the high binding energy side. The C 1s detail spectra (Figure S11b) are dominated by the contribution from conductive carbon, while the C–C/C–H peak of the PAA backbone has comparatively low intensity for all cycled samples. Interestingly, the C–O contribution for $\text{Li}_{0.7}\text{PAA}$ is reduced compared to the others, i.e., the development is reversed to the pristine samples. Finally, a new feature can be noted at 290.7 eV which is due to carbonate(s) as decomposition products coming from the electrolyte. The reduced C–O content for $\text{Li}_{0.7}\text{PAA}$ is also corroborated by the O 1s detail spectra (Figure S11c). The other peak in the O 1s spectra (at 531.8 eV) contains in addition to the C=O signal also the contribution from phosphate, which is the final decomposition product of the LiPF_6 electrolyte salt. The phosphate is also detected in the P 2p spectra (P 2p^{3/2} peak at 133.4 eV, Figure S11b). In addition, a further peak doublet due to partly decomposed LiPO_xF_y (P 2p^{3/2} peak at 136.2 eV) appears for all samples, while the signal of intact LiPF_6 (P 2p^{3/2} peak at 137.7 eV) is only found for the Li_0PAA sample. Correspondingly, the LiPF_6 peak (688.5 eV) is most clearly seen in the F 1s spectrum of the Li_0PAA sample, while its intensity is only small for the other two samples. The two other signals in the F 1s spectra (Figure S11d) can be assigned to LiPO_xF_y (687.1 eV) and LiF (685.0 eV), respectively. Most importantly, a successive increase of the LiF contribution with increasing neutralization is obvious. Therefore, it seems likely that the higher amount of Li^+ ions in partially neutralized PAA enables the decomposition of FEC. The higher ratio of inorganic SEI compounds like LiF, which is rather rigid, can be one reason for the improved cycle life, as it is less prone to be harmed during cycling and shows higher Li^+ ion conductivity, at the same time passivating the Si surface.^[42–45]

3. Conclusions

In summary, we have demonstrated how the partial neutralization of the PAA improves the processability of the pure silicon-based anode and also enhances the overall electrochemical and physicochemical properties of the synthesized anodes. Nevertheless, an excessive neutralization degree above 70% is not favorable, as it diminishes the battery cycle life and also gassing of the slurry occurred as a major challenge. Therefore, a simple increase in neutralization degree does not necessarily improve all the important properties and performance of the anode, but rather resembles the search of the best compromise. Additionally, higher SC during mixing changes electrode and electrochemical properties and gives improvement in cycle life. This influence needs further investigation in future studies to understand underlying mechanisms and dependencies between SC and neutralization degree. Furthermore, a detailed TEM-EELS and XPS analysis shows the interaction between Si particles and binder, as well as the polymer distribution within the electrodes. Overall, this work shows the outstanding performance of Si-dominant anodes with limitation of Si capacity by oversizing of the anode (high N/P ratio). It is important to note that the active material was only based on pure SiMPs. Additionally, the best performing cells showed the least degradation in SEM on electrode and particle level and indicated a different SEI composition with a higher contribution of stable inorganic LiF in the SEI. Literature shows that modification of the binder towards more stable and/or self-healing networks is crucial to stabilize the SiMP-based anode. Therefore, the partial neutralization of PAA should be taken into account when introducing crosslinkers. The use of multivalent cations can be an important benefit to gain self-healing properties without need for very complex binder systems. Also, as the capacity limitation plays a crucial role in further development of SiMPs-based anodes, experiments are ongoing which will show the impact of lower cutoff voltage variation.

Experimental Section/Methods

Experimental details are provided in the supporting information (SI).

Detailed description of the methods and instruments used in this work is provided in the Supporting Information.

Supporting Information Summary

Supporting Information is available from the Wiley Online Library or from the corresponding authors.

Experimental Section, SEM-EDX images of pristine and cycled electrodes, TEM-EELS images of pristine Li_0PAA and $\text{Li}_{0.3}\text{PAA}$ electrode, XPS survey and detail measurements of pristine and cycled electrodes based on Li_0PAA , $\text{Li}_{0.3}\text{PAA}$, $\text{Li}_{0.7}\text{PAA}$, half-cell C-rate test.

The following files are available free of charge.

Supporting Information (PDF).

Abbreviations

CB	carbon black
CCCV	constant current constant voltage
DCIR	direct current internal resistance
DMC	dimethyl carbonate
EC	ethylene carbonate
EDX	energy-dispersive X-ray spectroscopy
EELS	electron energy loss spectroscopy
EMC	ethyl-methyl carbonate
FCE	first cycle efficiency
FEC	fluoroethylene carbonate
FIB	focused ion beam
FTIR	Fourier-transform infrared spectroscopy
LIB	lithium ion battery
LiOH	lithium hydroxide
Li _x PAA	lithiated PAA to degree x
M _w	average molar mass
NMC811	lithium nickel manganese cobalt oxide (8:1:1)
N/P	negative to positive ratio
PAA	polyacrylic acid
PVDF	polyvinylidene fluoride
R2R	roll to roll
SC	solids content
SEI	solid electrolyte interphase
SEM	scanning electron microscopy
SIMP	silicon microparticle
SINP	silicon nanoparticle
SOH	state of health
SWCNTs	single-wall carbon nanotubes
TEM	transmission electron microscopy
VC	vinylene carbonate
wt.%	weight percent
XPS	X-ray photoelectron spectroscopy

Author Contributions

The manuscript was written through contributions of all authors. All authors have given approval to the final version of the manuscript.

Acknowledgements

We acknowledge the financial support of Mercedes-Benz AG, (Stuttgart, Germany). M.A. gratefully acknowledges the financial support from the Deutsche Forschungsgemeinschaft (DFG, German Research Foundation) under Germany's Excellence Strategy – EXC 2154 – Project number 390874152 (POLiS Cluster of Excellence). Financial support by Ulm University and the Helmholtz-Gemeinschaft (HGF) is gratefully acknowledged. G.K. thanks Philipp Bellucci from Mercedes-Benz AG for the preparation of FIB cross-sections of the samples and SEM/EDX measurements. Clementine Warres from NMI Tübingen is acknowledged for the lamella preparation and measurement of TEM-EELS spectra. This work contributes to the research performed at

CELEST (the Center for Electrochemical Energy Storage Ulm-Karlsruhe). Open Access funding enabled and organized by Projekt DEAL.

Conflict of Interests

The authors declare no conflict of interest.

Data Availability Statement

The data that support the findings of this study are available from the corresponding author upon reasonable request.

Keywords: Silicon anode • Micron-sized metallurgical silicon • Partially neutralized polyacrylic acid • Binder distribution • TEM-EELS

- [1] M. N. Obrovac, *Curr. Opin. Electrochem.* **2018**, *9*, 8–17.
- [2] K. Feng, M. Li, W. Liu, A. G. Kashkooli, X. Xiao, M. Cai, Z. Chen, *Small* **2018**, *14*, 1702737.
- [3] M. N. Obrovac, V. L. Chevrier, *Chem. Rev.* **2014**, *114*, 11444–11502.
- [4] M. Armand, P. Axmann, D. Bresser, M. Copley, K. Edström, C. Ekberg, D. Guyomard, B. Lestriez, P. Novák, M. Petranikova, W. Porcher, S. Trabesinger, M. Wohlfahrt-Mehrens, H. Zhang, *J. Power Sources* **2020**, *479*, 228708.
- [5] X. Zuo, J. Zhu, P. Müller-Buschbaum, Y.-J. Cheng, *Nano Energy* **2017**, *31*, 113–143.
- [6] C. Zhang, F. Wang, J. Han, S. Bai, J. Tan, J. Liu, F. Li, *Small Structures* **2021**, *2*, 2100009.
- [7] B. Zhu, G. Liu, G. Lv, Y. Mu, Y. Zhao, Y. Wang, X. Li, P. Yao, Y. Deng, Y. Cui, J. Zhu, *Sci. Adv.* **2019**, *5*, eaax0651.
- [8] Y. Li, X. Zheng, Z. Cao, Y. Wang, Y. Wang, L. Lv, W. Huang, Y. Huang, H. Zheng, *Energy Storage Mater.* **2023**, *55*, 660–668.
- [9] D. Rehnlund, F. Lindgren, S. Böhme, T. Nordh, Y. Zou, J. Pettersson, U. Bexell, M. Boman, K. Edström, L. Nyholm, *Energy Environ. Sci.* **2017**, *10*, 1350–1357.
- [10] X. Su, Q. Wu, J. Li, X. Xiao, A. Lott, W. Lu, B. W. Sheldon, J. Wu, *Adv. Energy Mater.* **2014**, *4*, 1300882.
- [11] G. G. Eshetu, H. Zhang, X. Judez, H. Adenusi, M. Armand, S. Passerini, E. Figgeimeier, *Nat. Commun.* **2021**, *12*, 5459.
- [12] F. Li, J. Xu, Z. Hou, M. Li, R. Yang, *ChemNanoMat* **2020**, *6*, 720–738.
- [13] H. Wu, Y. Cui, *Nano Today* **2012**, *7*, 414–429.
- [14] X. Zhao, V.-P. Lehto, *Nanotechnology* **2021**, *32*, 42002.
- [15] Y. Yang, W. Yuan, W. Kang, Y. Ye, Y. Yuan, Z. Qiu, C. Wang, X. Zhang, Y. Ke, Y. Tang, *Nanoscale* **2020**, *12*, 7461–7484.
- [16] X. H. Liu, L. Zhong, S. Huang, S. X. Mao, T. Zhu, J. Y. Huang, *ACS Nano* **2012**, *6*, 1522–1531.
- [17] G. Zhu, D. Chao, W. Xu, M. Wu, H. Zhang, *ACS Nano* **2021**, *15*, 15567–15593.
- [18] F. Zou, A. Manthiram, *Adv. Energy Mater.* **2020**, *10*, 2002508.
- [19] Y.-M. Zhao, F.-S. Yue, S.-C. Li, Y. Zhang, Z.-R. Tian, Q. Xu, S. Xin, Y.-G. Guo, *InfoMat* **2021**, *3*, 460–501.
- [20] G. G. Eshetu, E. Figgeimeier, *ChemSusChem* **2019**, *12*, 2515–2539.
- [21] J.-T. Li, Z.-Y. Wu, Y.-Q. Lu, Y. Zhou, Q.-S. Huang, L. Huang, S.-G. Sun, *Adv. Energy Mater.* **2017**, *7*, 1701185.
- [22] D. Bresser, D. Buchholz, A. Moretti, A. Varzi, S. Passerini, *Energy Environ. Sci.* **2018**, *11*, 3096–3127.
- [23] J. Xiong, N. Dupré, D. Mazouzi, D. Guyomard, L. Roué, B. Lestriez, *ACS Appl. Mater. Interfaces* **2021**, *13*, 28304–28323.
- [24] K. A. Hays, R. E. Ruther, A. J. Kukay, P. Cao, T. Saito, D. L. Wood, J. Li, *J. Power Sources* **2018**, *384*, 136–144.
- [25] Z. Li, W. Tang, Y. Yang, G. Lai, Z. Lin, H. Xiao, J. Qiu, X. Wei, S. Wu, Z. Lin, *Adv. Funct. Mater.* **2022**, *32*, 2206615.
- [26] D. Dang, Y. Wang, M. Wang, J. Hu, C. Ban, Y.-T. Cheng, *ACS Appl. Energ. Mater.* **2020**, *3*, 10940–10949.

- [27] N. Hamzelui, G. G. Eshetu, E. Figgemeier, *J. Energy Storage* **2021**, *35*, 102098.
- [28] M.-T. F. Rodrigues, S. E. Trask, I. A. Shkrob, D. P. Abraham, *J. Power Sources* **2018**, *395*, 289–294.
- [29] K. A. Hays, B. Key, J. Li, D. L. Wood, G. M. Veith, *J. Phys. Chem. C* **2018**, *122*, 9746–9754.
- [30] B. Hu, S. Jiang, I. A. Shkrob, J. Zhang, S. E. Trask, B. J. Polzin, A. Jansen, W. Chen, C. Liao, Z. Zhang, L. Zhang, *J. Power Sources* **2019**, *416*, 125–131.
- [31] Z.-J. Han, K. Yamagiwa, N. Yabuuchi, J.-Y. Son, Y.-T. Cui, H. Oji, A. Kogure, T. Harada, S. Ishikawa, Y. Aoki, S. Komaba, *Phys. Chem. Chem. Phys.* **2015**, *17*, 3783–3795.
- [32] M. K. Burdette-Trofimov, B. L. Armstrong, A. M. Rogers, L. Heroux, M. Doucet, G. Yang, N. D. Phillip, M. K. Kidder, G. M. Veith, *J. Phys. Chem. C* **2020**, *124*, 13479–13494.
- [33] Z.-Y. Wu, L. Deng, J.-T. Li, S. Zanna, A. Seyeux, L. Huang, S.-G. Sun, P. Marcus, J. Świątowska, *Batteries* **2022**, *8*, 271.
- [34] C. C. Nguyen, T. Yoon, D. M. Seo, P. Guduru, B. L. Lucht, *ACS Appl. Mater. Interfaces* **2016**, *8*, 12211–12220.
- [35] J. He, C. Das, F. Yang, J. Maibach, *Electrochim. Acta* **2022**, *411*, 140038.
- [36] T. R. Martin, R. T. Pekarek, J. E. Coyle, M. C. Schulze, N. R. Neale, *J. Mater. Chem. A* **2021**, *9*, 21929–21938.
- [37] W. Porcher, S. Chazelle, A. Boulineau, N. Mariage, J. P. Alper, T. van Rompaey, J.-S. Bridel, C. Haon, *J. Electrochem. Soc.* **2017**, *164*, A3633–A3640.
- [38] R. Nölle, K. Beltrop, F. Holtstiege, J. Kasnatscheew, T. Placke, M. Winter, *Mater. Today* **2020**, *32*, 131–146.
- [39] F. Maroni, M. Spreafico, A. Schönecker, M. Wohlfahrt-Mehrens, M. Marinaro, *J. Electrochem. Soc.* **2022**, *169*, 80506.
- [40] N. P. Wagner, K. Asheim, F. Vullum-Bruer, A. M. Svensson, *J. Power Sources* **2019**, *437*, 226884.
- [41] F. Reuter, A. Baasner, J. Pampel, M. Piwko, S. Dörfler, H. Althues, S. Kaskel, *J. Electrochem. Soc.* **2019**, *166*, A3265–A3271.
- [42] X.-Q. Zhang, X.-B. Cheng, X. Chen, C. Yan, Q. Zhang, *Adv. Funct. Mater.* **2017**, *27*, 1605989.
- [43] T. Jia, G. Zhong, S. Lu, X. Ren, Y. Lv, N. Li, R. Yin, G. Kang, K. Cai, F. Kang, Y. Cao, *Chem. Eng. J.* **2023**, *454*, 140397.
- [44] P. Parikh, M. Sina, A. Banerjee, X. Wang, M. S. D’Souza, J.-M. Doux, E. A. Wu, O. Y. Trieu, Y. Gong, Q. Zhou, K. Snyder, Y. S. Meng, *Chem. Mater.* **2019**, *31*, 2535–2544.
- [45] H. Shin, J. Park, S. Han, A. M. Sastry, W. Lu, *J. Power Sources* **2015**, *277*, 169–179.

Manuscript received: May 17, 2024

Revised manuscript received: June 27, 2024

Accepted manuscript online: July 11, 2024

Version of record online: September 3, 2024